# Supplementary material

## Mechanisms of size effects in elastic architected solids

Sahin Celik[1], Hao Yin[2], Ivan Grega[2], Ankit Srivastava[1,*], Vikram S. Deshpande[2,*]

[1]Department of Materials Science and Engineering, Texas A&M University, College Station, TX 77843, USA
[2]Department of Engineering, University of Cambridge, Cambridge, CB2 1PZ, U.K.

*Corresponding authors: ankit.sri@tamu.edu (AS), vsd20@cam.ac.uk (VSD)

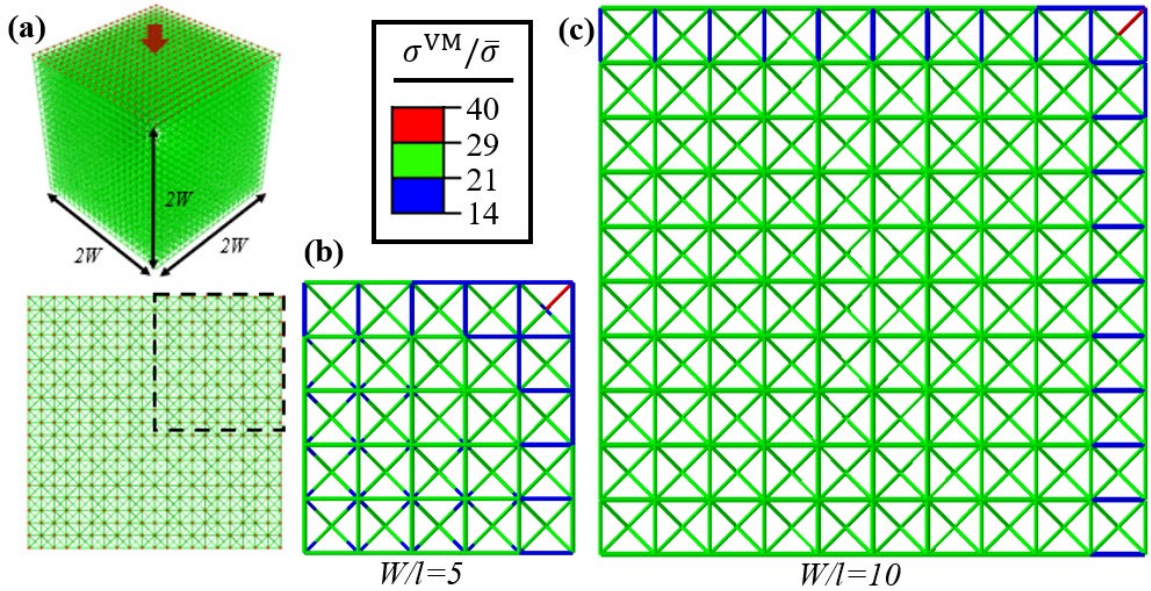



**Figure S1. (a)** Lattice specimen under uniaxial loading, together with a top view of the specimen showing the highlighted quarter region over which the strut-level von Mises stress distribution, $\sigma^{\mathrm{VM}}$, is plotted. Distributions of strut-level von Mises stress normalized by $\bar{\sigma} = F/(2W)^2$, where $F$ is the total reaction force on the loaded surface, are shown for BCC/SC specimens with **(b)** $W/l = 5$ and **(c)** $W/l = 10$, as predicted by full-field finite element calculations.

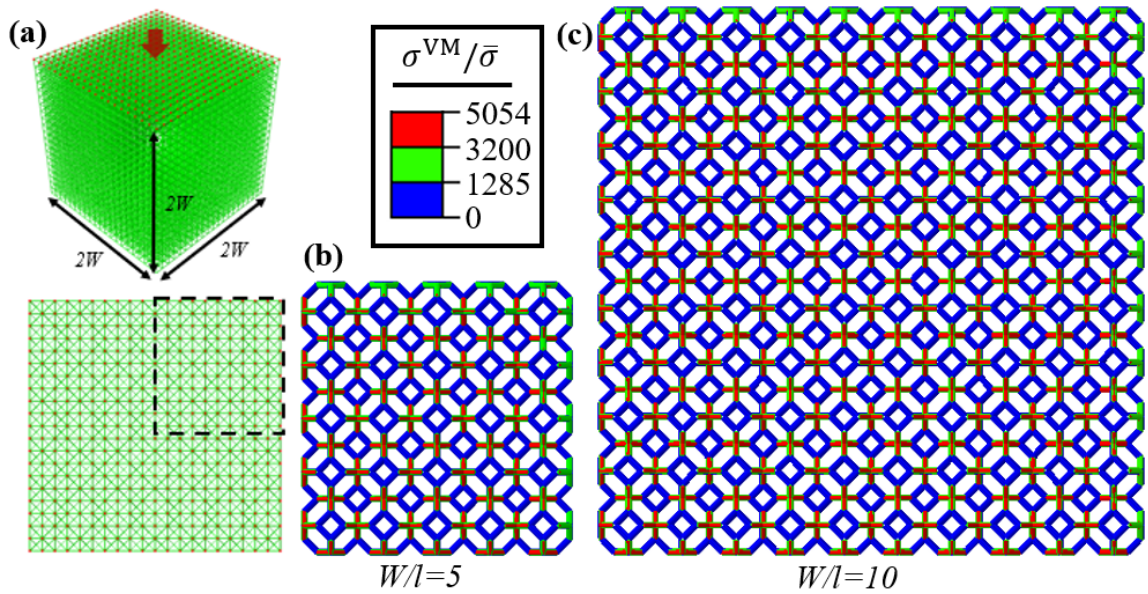



**Figure S2. (a)** Lattice specimen under uniaxial loading, together with a top view of the specimen showing the highlighted quarter region over which the strut-level von Mises stress distribution, $\sigma^{VM}$, is plotted. Distributions of strut-level von Mises stress normalized by $\bar{\sigma} = F/(2W)^2$, where $F$ is the total reaction force on the loaded surface, are shown for Kelvin specimens with **(b)** $W/l = 5$ and **(c)** $W/l = 10$, as predicted by full-field finite element calculations.

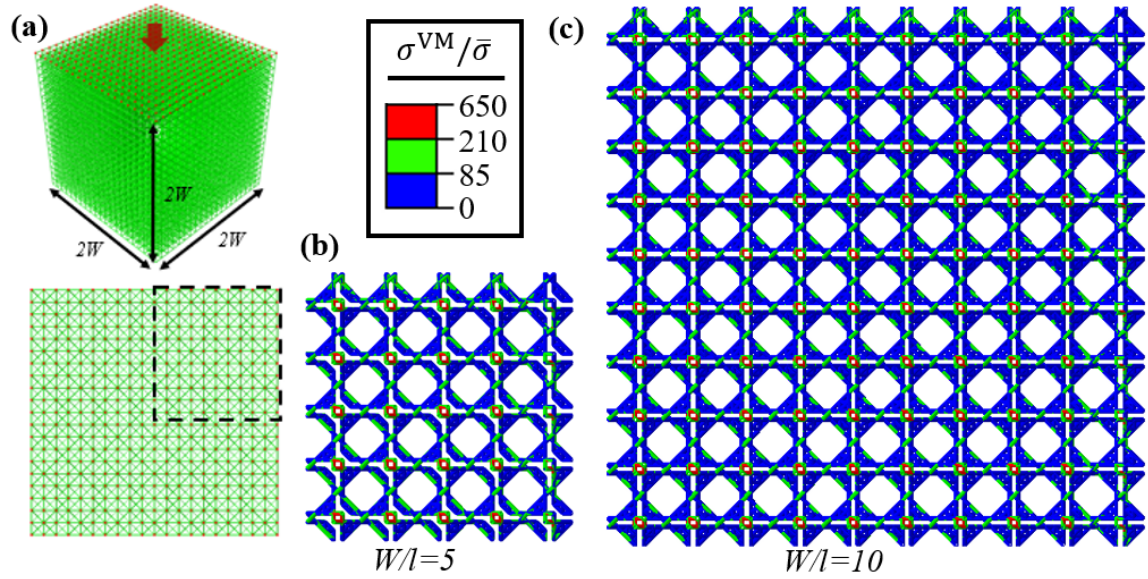



**Figure S3. (a)** Lattice specimen under uniaxial loading, together with a top view of the specimen showing the highlighted quarter region over which the strut-level von Mises stress distribution, $\sigma^{VM}$, is plotted. Distributions of strut-level von Mises stress normalized by $\bar{\sigma} = F/(2W)^2$, where $F$ is the total reaction force on the loaded surface, are shown for E11128 specimens with **(b)** $W/l = 5$ and **(c)** $W/l = 10$, as predicted by full-field finite element calculations.

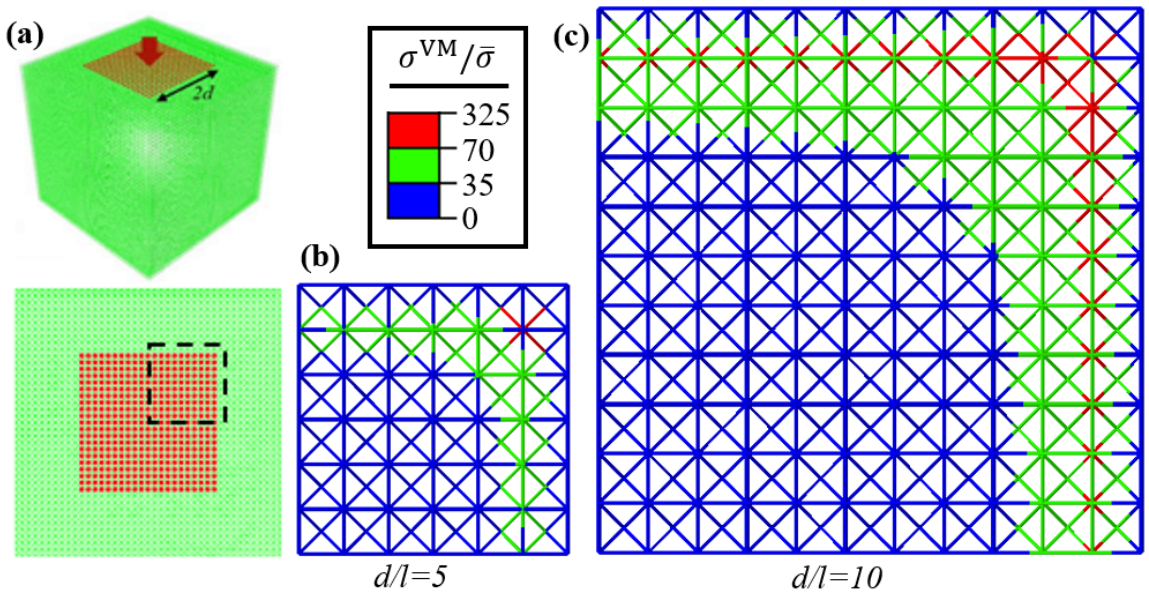



**Figure S4. (a)** Lattice specimen under indentation, together with a top view of the specimen showing the highlighted region over which the strut-level von Mises stress distribution, $\sigma^{VM}$, is plotted. Distributions of strut-level von Mises stress normalized by $\bar{\sigma} = P/(2d)^2$, where $P$ is the total indentation reaction load, are shown for BCC/SC specimens with **(b)** $d/l = 5$ and **(c)** $d/l = 10$, as predicted by full-field finite element calculations.

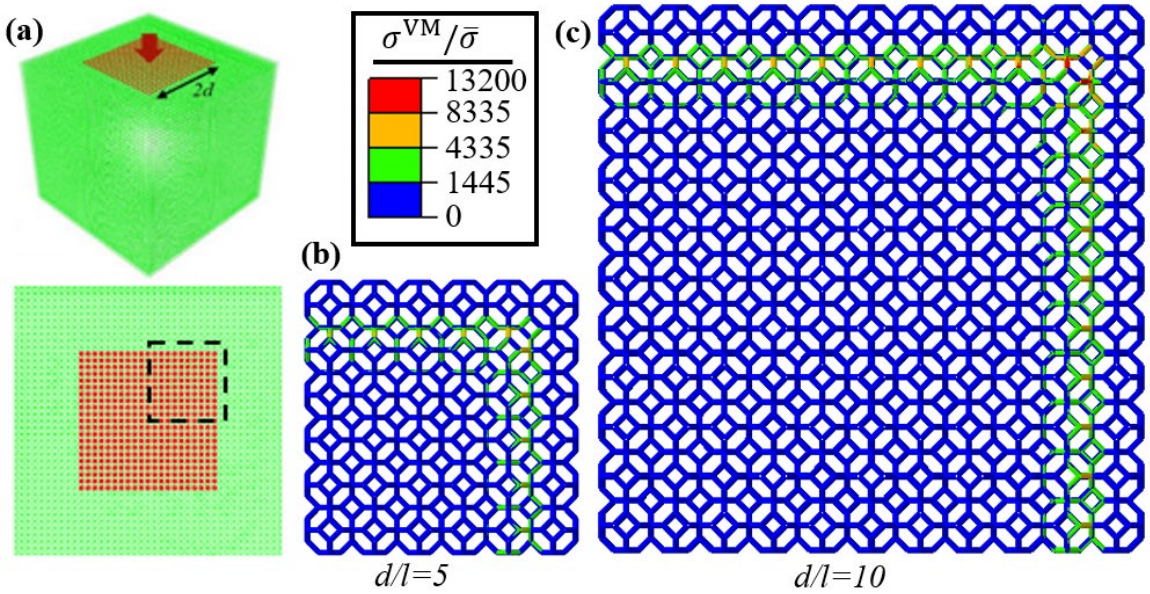



**Figure S5. (a)** Lattice specimen under indentation, together with a top view of the specimen showing the highlighted region over which the strut-level von Mises stress distribution, $\sigma^{VM}$, is plotted. Distributions of strut-level von Mises stress normalized by $\bar{\sigma} = P/(2d)^2$, where $P$ is the total indentation reaction load, are shown for Kelvin specimens with **(b)** $d/l = 5$ and **(c)** $d/l = 10$, as predicted by full-field finite element calculations.

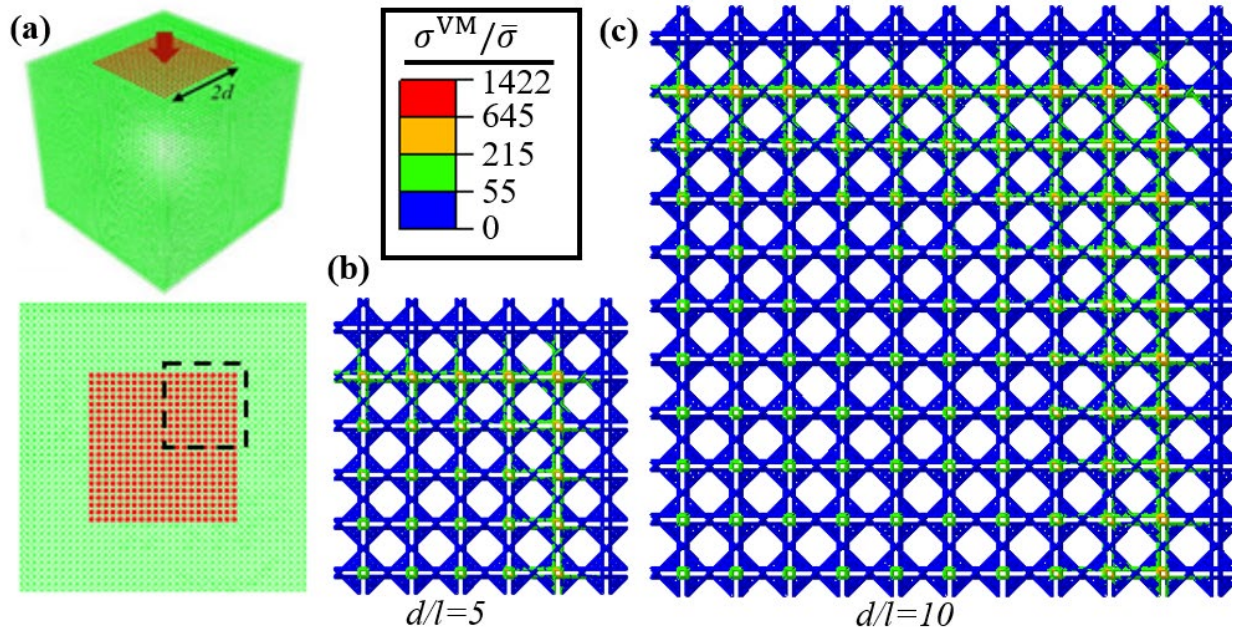



**Figure S6. (a)** Lattice specimen under indentation, together with a top view of the specimen showing the highlighted region over which the strut-level von Mises stress distribution, $\sigma^{\mathrm{VM}}$, is plotted. Distributions of strut-level von Mises stress normalized by $\bar{\sigma} = P/(2d)^2$, where P is the total indentation reaction load, are shown for E11128 specimens with **(b)** $W/l = 5$ and **(c)** $W/l = 10$, as predicted by full-field finite element calculations.

## Section S1: Affine upper-bound model for the BCC/SC lattice

The affine upper-bound response of the BCC/SC lattice under uniaxial compression in the $x_2$-direction is obtained using an energy-based unit-cell formulation. The BCC/SC architecture is stretching dominated; therefore, each strut is modeled as a pin-jointed truss member carrying only axial deformation. A macroscopic strain $\varepsilon$ is applied in the $x_2$-direction, and the strain energy stored in each strut is evaluated under the corresponding affine deformation. Due to the symmetry of the unit cell, struts with identical strain energy are grouped into three representative sets, as shown in Fig. S7: vertical simple-cubic struts, horizontal simple-cubic struts, and inclined BCC struts.




**Figure S7.** BCC/SC unit cell used in the affine upper-bound model. The struts are grouped into: vertical simple-cubic struts ($s_1$) aligned with the loading direction, horizontal simple-cubic struts ($s_2$) transverse to the loading direction, and inclined BCC struts. Struts within each group have identical axial strain under the imposed affine deformation.

The total strain energy of the unit cell is written as

$$\Pi = \Pi_1 + \Pi_2 + \Pi_3, \tag{S1}$$

where $\Pi_1$, $\Pi_2$, and $\Pi_3$ are the energy contributions from the vertical simple-cubic struts, horizontal simple-cubic struts, and inclined BCC struts, respectively. The corresponding strain-energy density is

$$U = \frac{\Pi}{l^3}. \tag{S2}$$

For the imposed affine strain field, the transverse strains satisfy $\varepsilon_{11} = \varepsilon_{33}$. The vertical simple-cubic struts aligned with the loading direction have axial strain $\varepsilon_{22}$, the horizontal simple-cubic struts transverse to the loading direction have axial strain $\varepsilon_{11}$, and the inclined BCC struts have axial strain $(2\varepsilon_{11} + \varepsilon_{22})/3$. Thus,

$$\Pi_1 = 2f_1 E_s \pi a_1^2 l \varepsilon_{22}^2, \tag{S3}$$

$$\Pi_2 = 4f_2 E_s \pi a_1^2 l \varepsilon_{11}^2, \tag{S4}$$

and

$$\Pi_3 = 4\frac{\sqrt{3}}{2} E_s \pi a_2^2 l \left(\frac{2\varepsilon_{11}+\varepsilon_{22}}{3}\right)^2. \tag{S5}$$

Here, $a_1$ is the radius of the simple-cubic struts, $a_2$ is the radius of the inclined BCC struts, $E_s$ is the Young's modulus of the parent solid, and $l$ is the unit-cell length. The factors $f_1$ and $f_2$ account for the finite-size dependence of the effective number of simple-cubic struts per unit cell. As illustrated in Fig. S8, they are defined as

$$f_1 = \frac{N_{s1}}{4N_u^3}, \qquad f_2 = \frac{N_{s2}}{8N_u^3}, \tag{S6}$$

where $N_{s1}$ and $N_{s2}$ are the total numbers of vertical and horizontal simple-cubic struts in the finite specimen, respectively, and $N_u$ is the number of unit cells along each specimen edge.

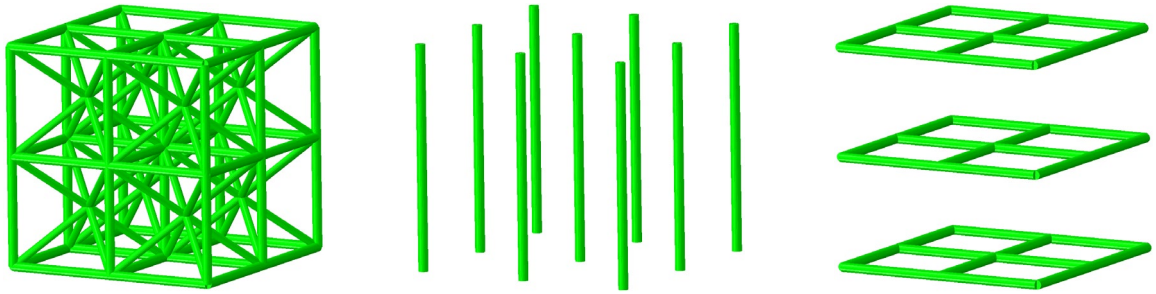


**Figure S8.** Illustration of the strut-counting procedure used to determine the fractional strut numbers $f_1$ and $f_2$ for a finite $(2 \times 2 \times 2)$ BCC/SC specimen.

Substituting Eqs. (S3)–(S5) into Eq. (S2) gives

$$U = \frac{E_s \pi}{l^2}\left[2f_1 a_1^2 \varepsilon_{22}^2 + 4f_2 a_1^2 \varepsilon_{11}^2 + \frac{2\sqrt{3}}{9} a_2^2 (2\varepsilon_{11} + \varepsilon_{22})^2\right]. \tag{S7}$$

For the BCC/SC lattice considered here, the ratio between the simple-cubic and inclined BCC strut radii is chosen as

$$\left(\frac{a_1}{a_2}\right)^2 = \frac{8\sqrt{3}}{9}, \tag{S8}$$

to ensure an elastically isotropic response. Using Eq. (S8), Eq. (S7) becomes

$$U = \frac{E_s \pi a_2^2}{l^2}\left[\frac{16\sqrt{3}}{9} f_1 \varepsilon_{22}^2 + \frac{32\sqrt{3}}{9} f_2 \varepsilon_{11}^2 + \frac{2\sqrt{3}}{9}(2\varepsilon_{11} + \varepsilon_{22})^2\right]. \tag{S9}$$

The relative density of the BCC/SC lattice is

$$\bar{\rho} = \frac{20\sqrt{3}\pi}{3}\left(\frac{a_2}{l}\right)^2. \tag{S10}$$

Therefore, Eq. (S9) can be rewritten as

$$U = E_s \bar{\rho}\left[\frac{4}{15} f_1 \varepsilon_{22}^2 + \frac{8}{15} f_2 \varepsilon_{11}^2 + \frac{1}{30}(2\varepsilon_{11} + \varepsilon_{22})^2\right]. \tag{S11}$$

The transverse strain is written as

$$\varepsilon_{11} = \varepsilon_{33} = -\nu\varepsilon_{22}. \tag{S12}$$

Using Eq. (S11), the strain-energy density becomes

$$U = E_s\bar{\rho}\varepsilon_{22}^2\left[\frac{4}{15}f_1 + \frac{8}{15}f_2\nu^2 + \frac{1}{30}(1-2\nu)^2\right]. \tag{S13}$$

The axial stress is obtained by differentiating Eq. (S13) with respect to $\varepsilon_{22}$:

$$\sigma_{22} = \frac{\partial U}{\partial \varepsilon_{22}} = E_s\bar{\rho}\varepsilon_{22}\left[\frac{8}{15}(f_1 + 2\nu^2 f_2) + \frac{1}{15}(1-2\nu)^2\right]. \tag{S14}$$

Therefore, the uniaxial stiffness is then given as

$$K_U = \frac{\sigma_{22}}{\varepsilon_{22}} = E_s\bar{\rho}\left[\frac{8}{15}(f_1 + 2\nu^2 f_2) + \frac{1}{15}(1-2\nu)^2\right]. \tag{S15}$$

The effective Poisson's ratio is obtained by enforcing the transverse stress-free condition.

$$\sigma_{11} = \frac{\partial U}{\partial \varepsilon_{11}} = E_s\bar{\rho}\left[\frac{4}{30}(2\varepsilon_{11} + \varepsilon_{22}) + \frac{8}{30}(4f_2\varepsilon_{11})\right] = 0, \tag{S16}$$

which gives,

$$\nu = -\frac{\varepsilon_{11}}{\varepsilon_{22}} = \frac{1}{2+8f_2}. \tag{S17}$$

**Section S2: Affine upper-bound model for the octet-truss lattice**

The affine upper-bound response of the octet-truss lattice under uniaxial compression in the $x_2$-direction is obtained using the same energy-based formulation as for the BCC/SC lattice. Since the octet-truss architecture is stretching dominated as well, each strut is again modeled as a pin-jointed truss member carrying only axial deformation. A macroscopic strain is imposed in the $x_2$-direction, and the strain energy stored in each strut is evaluated under the corresponding affine deformation. Owing to the symmetry of the unit cell, struts with identical strain energy are grouped into four representative sets, as shown in Fig. S9: vertical side-face struts, horizontal top and bottom cross struts, inclined interior struts, and horizontal interior struts.

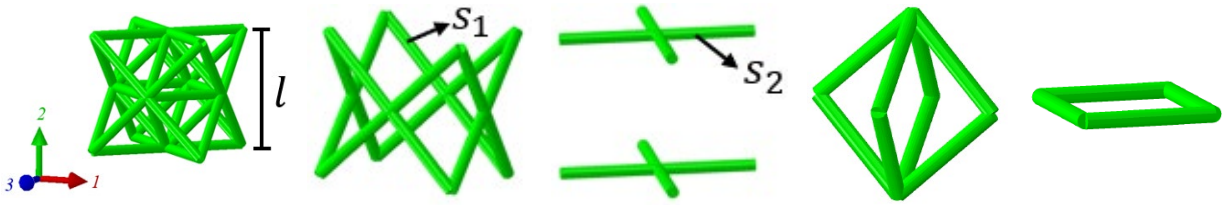



**Figure S9.** Octet-truss unit cell used in the affine upper-bound model. The struts are separated into four groups: vertical side-face struts, $s_1$, horizontal top and bottom cross struts, $s_2$, inclined interior struts, and horizontal interior struts. Struts within each group have identical axial strain under the imposed affine deformation.

The total strain energy of the unit cell is written as

$$\Pi = \Pi_1 + \Pi_2 + \Pi_3 + \Pi_4, \tag{S18}$$

and the corresponding strain-energy density is

$$U = \frac{\Pi}{l^3}. \tag{S19}$$

The strain-energy contributions of the four strut groups shown in Fig. S9 are

$$\Pi_1 = 2f_1 E_s \pi a^2 \frac{l}{\sqrt{2}} (\varepsilon_{11} + \varepsilon_{22})^2, \tag{S20}$$

$$\Pi_2 = 4f_2 E_s \pi a^2 \frac{l}{\sqrt{2}} \varepsilon_{11}^2, \tag{S21}$$

$$\Pi_3 = E_s \pi a^2 \frac{l}{\sqrt{2}} (\varepsilon_{11} + \varepsilon_{22})^2, \tag{S22}$$

and

$$\Pi_4 = 2E_s \pi a^2 \frac{l}{\sqrt{2}} \varepsilon_{11}^2. \tag{S23}$$

Here, $a$ is the common strut radius, $E_s$ is the Young's modulus of the parent solid, and $l$ is the unit-cell length. The factors $f_1$ and $f_2$ account for the finite-size dependence of the effective number of shared struts per unit cell. As illustrated in Fig. S10, they are defined as

$$f_1 = \frac{N_{s1}}{16N_u^3}, \qquad f_2 = \frac{N_{s2}}{8N_u^3}, \tag{S24}$$

Where $N_{s1}$ and $N_{s2}$ are the total number of vertical side-face struts and horizontal top/bottom cross struts in the finite specimen, respectively, and $N_u$ is the number of unit cells along each specimen edge.

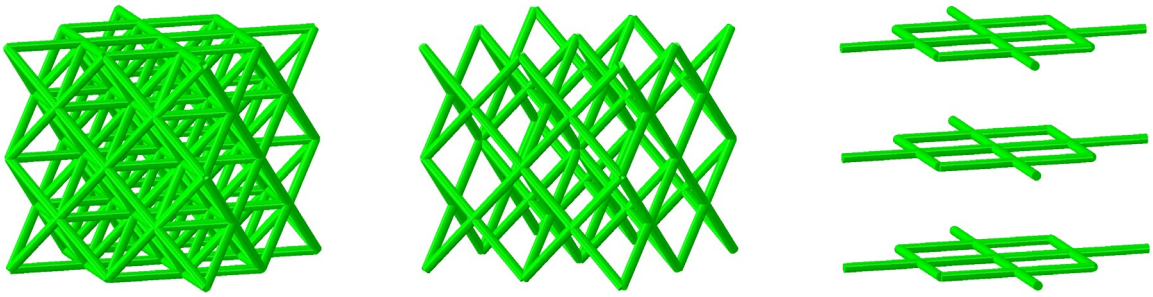


**Figure S10.** Illustration of the strut-counting procedure used to determine the fractional strut numbers $f_1$ and $f_2$ for a finite $(2 \times 2 \times 2)$ octet-truss lattice specimen.

Substituting Eqs. (S20)–(S23) into Eq. (S19) gives

$$U = \frac{1}{12} E_s 6\sqrt{2} \left(\frac{\pi a^2}{l^2}\right) [4f_2\varepsilon_{11}^2 + 2f_1(\varepsilon_{11} + \varepsilon_{22})^2 + (\varepsilon_{11} + \varepsilon_{22})^2 + 2\varepsilon_{11}^2]. \quad \text{(S25)}$$

Using the relative-density expression for the octet-truss lattice,

$$\bar{\rho} = 6\sqrt{2} \left(\frac{\pi a^2}{l^2}\right), \quad \text{(S26)}$$

Eq. (S25) can be written as

$$U = \frac{E_s \bar{\rho}}{12} [4f_2\varepsilon_{11}^2 + 2f_1(\varepsilon_{11} + \varepsilon_{22})^2 + (\varepsilon_{11} + \varepsilon_{22})^2 + 2\varepsilon_{11}^2]. \quad \text{(S27)}$$

The transverse strain relation is

$$\varepsilon_{11} = -\nu\varepsilon_{22}. \quad \text{(S28)}$$

Substituting Eq. (S28) into Eq. (S27) gives

$$U = \frac{E_s \bar{\rho}}{12} [4f_2\nu^2 + 2f_1(1-\nu)^2 + (1-\nu)^2 + 2\nu^2]\varepsilon_{22}^2. \quad \text{(S29)}$$

Equivalently,

$$U = \frac{E_s \bar{\rho}}{12} [(4f_2 + 2f_1 + 3)\nu^2 - (4f_1 + 2)\nu + 2f_1 + 1]\varepsilon_{22}^2. \quad \text{(S30)}$$

The axial stress is obtained by differentiating Eq. (S30) with respect to the applied strain:

$$\sigma_{22} = \frac{\partial U}{\partial \varepsilon_{22}} = \frac{E_s \bar{\rho}}{6} [(4f_2 + 2f_1 + 3)\nu^2 - (4f_1 + 2)\nu + 2f_1 + 1]\varepsilon_{22}. \quad \text{(S31)}$$

Thus, the effective axial stiffness is

$$K_U = \frac{E_S\bar{\rho}}{6}[(4f_2 + 2f_1 + 3)\nu^2 - (4f_1 + 2)\nu + 2f_1 + 1]. \quad \text{(S32)}$$

The effective Poisson's ratio is obtained by enforcing the transverse stress-free condition. Since uniaxial compression is applied in the $x_2$-direction, the transverse stress in the $x_1$-direction must vanish:

$$\sigma_{11} = \frac{\partial U}{\partial \varepsilon_{11}} = 0. \quad \text{(S33)}$$

This gives,

$$\nu = -\frac{\varepsilon_{11}}{\varepsilon_{22}} = \frac{4f_1+2}{8f_2+4f_1+6}. \quad \text{(S34)}$$